RSC Advances

ROYAL SOCIETY OF CHEMISTRY

www.rsc.org/advances

RSC Advances

ARTICLE

Schiff-Base Polymers Derived Nitrogen-Rich Microporous Carbon Spheres Synthesized by Molten-Salt Route for High-performance Supercapacitors

Received 00th January 20xx,
Accepted 00th January 20xx

DOI: 10.1039/x0xx00000x

www.rsc.org/

Shanjin Su,[a] Qingxue Lai,[a] and Yanyu Liang*[a]

Nitrogen-rich microporous carbon spheres (NMCSs) have been prepared *via* thermal treatment of Schiff-base polymer monomers of melamine and terephthalaldehyde in the presence of molten-salt $ZnCl_2$/KCl system. The use of $ZnCl_2$ and KCl in the reaction allows for NMCSs with a high specific surface area of 1929 m^2 g^{-1} and pore volume of 0.85 cm^3 g^{-1}, respectively. More importantly, most of the pore volume is contributed by micropores, which are ideal as an electrode for high-performance supercapacitors. When tested as supercapacitor electrodes, NMCSs delivered an excellent specific capacitance of 365 F g^{-1} at a current density of 0.5 A g^{-1} and it still maintained 230 F g^{-1} even at 10 A g^{-1}. Moreover, a very stable cycle life of 94% capacitance retention was observed after 10000 charge-discharge cycles at a current density of 3 A g^{-1}. With regard to the inexpensive precursors, simple and environmental-friendly synthetic route, this novel molten salt strategy holds great potential for the industrial manufacture of NMCSs for usage in energy storage and convention.

1. Introduction

Searching for novel, environmental-friendly, low-cost, and high-performance energy storage devices is under great demand nowadays.[1-3] Supercapacitors also known as electrochemical capacitors or ultracapacitors are considered to be very attractive due to their high power density, fast charge-discharge rate, long cycle life and wide operational temperature range.[2] Thus, they are rapidly being adopted for a wide range of electrical energy storage applications such as back-up systems, consumer electronics, uninterruptible power sources, and hybrid electric vehicles, *etc*.[4] Based on the energy storage mechanism, supercapacitors are generally divided into electrical double layer capacitors (EDLCs) and pseudocapacitors.[2] EDLCs store energy based on the accumulation of charge in the double layer formed on the surface of inert electrodes. In contrast, pseudocapacitors store energy via fast and reversible redox reactions that occur on the surface of the active material. Generally, EDLCs have higher power density and longer cyclic life than pseudocapacitors.[5] However, the practical applications of EDLCs is still limited by their low energy density owing to relatively low capacitance of EDLCs,[6] which is strongly dependent on the surface area and pore size distribution of the electrode materials. In this regard, research to improve the performance of electrode materials has dramatically increased.

Carbonaceous materials, such as activated carbon,[7] carbon nanotubes,[8] and graphene[9-11] have been widely used as electrode materials for EDLCs in view of their high surface areas as well as good conductivity. Doping of heteroatom (such as O, N and B) can effectively afford the extra pseudocapacitance, therefore, improving the capacitance performance of these materials.[12-14] Many approaches like activation methods,[6, 15] nanocasting,[16] molten-salt route[17] and direct pyrolysis of polymers *etc*.[18] have been employed to prepare nitrogen-doped porous carbons (NPCs). A variety of nitrogen-containing carbon precursors including ionic liquids,[17, 19] biomass,[20, 21] synthetic polymers[22, 23] *etc*. have been attempted to build up NPCs. As synthetic polymers, Schiff-base porous polymers have attracted tremendous attention on account of their porous features and high nitrogen content, making them ideally promising candidates in the synthesis of NPCs. Recently, Zhuang and co-workers[24] reported nitrogen-enriched porous carbon nanosheets using Schiff-base polymers as nitrogen-containing carbon precursors and graphene as a 2D template. The resultant NPCs material exhibited a high specific capacitance of 424 F g^{-1} at the current density of 0.1 A g^{-1} in 6 M KOH aqueous solution. However, the preparation process of Schiff-base polymers through refluxing in dimethyl sulfoxide under an inert atmosphere for 3 days is so complicated, high-cost and time-consuming, apparently, it is unsuitable for large-scale production and industrial applications.

[a] *College of Materials Science and Technology, Nanjing University of Aeronautics and Astronautics, Nanjing, 210016 (P.R. China); Fax: +86-025-52112626; Tel: +86-025-52112626; E-mail: liangyy403@126.com*

† Electronic Supplementary Information (ESI) available: [details of additional experiment data are available]. See DOI: 10.1039/x0xx00000x

In the last few years, molten-salt route has been viewed as a simple and green approach to prepare porous carbon materials. It has distinctive advantages over conventional liquid phase synthesis, hard and soft templating methods and activation methods.[17, 25] Herein, molten-salt route and Schiff-base chemistry are combined for preparation of nitrogen-rich microporous carbon spheres (NMCSs). By directly thermal treatment of Schiff-base polymer monomers of melamine and terephthalaldehyde (TPAL) in molten $ZnCl_2$/KCl system (melting point 230 °C), NMCSs with well-defined microporosity and moderate nitrogen content were obtained, as shown in Scheme 1**.** Electrochemical measurements indicate that the as-prepared NMCSs show excellent capacitive performance (365 F g^{-1} at 0.5 A g^{-1}) in an alkaline environment as well as very stable cycle life.

2. Experimental Section

2.1 Synthesis

In a typical synthesis of the NMCSs, melamine (125 mg) and TPAL (200 mg) powder were mixed with $ZnCl_2$ (1 g) and KCl (0.3 g), then the mixture were ground in an agate mortar for 3 minutes before the following calcination process. The sample of NPC1-ZK(0, 0) was prepared under the same condition without adding of $ZnCl_2$ and KCl. Other samples were also synthesized by adjusting the weight ratio of $ZnCl_2$ to KCl, which are NPC2-ZK(1, 0): ($ZnCl_2$ 1 g, KCl 0 g), NMCSs1-ZK(2, 1): ($ZnCl_2$ 2 g, KCl 1 g), NPC3-ZK(6, 3) ($ZnCl_2$ 6 g, KCl 3 g) and NPC4-ZK(0, 1) : ($ZnCl_2$ 0 g, KCl 1 g) respectively. Then, the as-prepared mixtures were placed in a ceramic crucible and heated to 700 °C with an increasing rate of 2 °C min^{-1}. After holding this temperature for 2 h, the samples were allowed to cool down to room temperature. All steps were carried out under a constant flow of nitrogen. In order to remove the residual salt, the samples were ground and washed in 2 M HCl and distilled water to remove any metal residue and finally filtrated and dried in vacuum.

2.2 Characterization

The structural and morphological characterizations were performed by scanning electron microscopy (SEM, XL-30ESEM), transmission electron microscopy (TEM, JEM-200CX), Fourier transform infrared spectrometry (FT-IR, Nicolet 750), X-ray photoelectron spectroscopy (XPS, Perkin-Elmer PHI 550 spectrometer with Al Ka as the X-ray source.) and Raman spectroscopy (Renishaw (in Via), England). The N_2 adsorption/desorption tests were performed by BET measurements using an ASAP-2020 surface area analyzer.

2.3 Electrochemical Measurements

The electrochemical measurements were carried out on a CHI 660E electrochemical workstation in a 6 M KOH aqueous electrolyte at room temperature using a three electrode system. A platinum wire and a saturated calomel electrode (SCE) electrode were used as the counter and reference electrode, respectively. The working electrode was prepared by mixing 80 wt% active material (5 mg) with 10 wt% acetylene black and 10 wt% polytetrafluoroethylene (PTFE) binder dispersed in ethanol solvent to form a slurry, then the slurry was pressed on a nickel foam serving as a current collector and dried in vacuum oven at 60 °C for 10 h. The cycling performance test was carried out with a CT2001D tester (Wuhan, China).

3. Results and Discussion

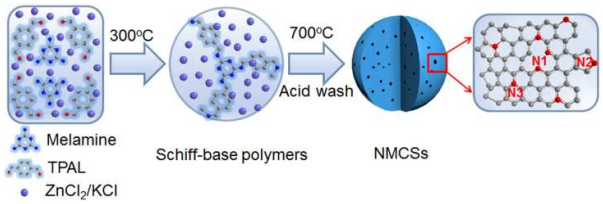

Scheme 1. Schematic illustration of the fabrication of NMCSs.

The synthetic procedures for the formation of NMCSs are shown in Scheme 1. Firstly, Schiff-base polymers were formed by the reaction of melamine and TPAL with increasing of the temperature (Figure S1). Then, as the temperature continued to rise, the polymer was carbonized and activated to the formation of NMCSs. The morphology and microstructure of the resultant NMCSs were investigated by scanning electron microscopy (SEM), transmission electron microscopy (TEM), Raman spectroscopy and nitrogen adsorption-desorption analysis. The SEM image shown in Figure 1c clearly indicates that NMCSs are composed of regular spheres with the diameter of 300-400 nm in size, which are connected to each other. On the other hand, no well-defined spheres were observed in the SEM images of NPC1-ZK(0, 0), NPC2-ZK(1, 0) (Figure 1a-b) and NPC4-ZK(0, 1) (Figure S2b). Therefore, the formation of spherical morphology is considered to be due to the combined effect of $ZnCl_2$ and KCl, as carbon disperses only in the KCl phase proposed by previous report,[26] and the individual KCl can't be melted in 700°C without the adding of $ZnCl_2$. As the mass ratio of KCl increased, the tendency of forming spherical morphology grows (Figure 1d). However, when too much $ZnCl_2$ and KCl were added, the spherical morphology disappeared (Figure S2a). Figure 1e and Figure 1f are TEM images of NMCSs. As shown in Figure 1e, the spherical morphology of NMCSs is well consistent with SEM observation. Many interconnected nanopores with the pore size less than 5 nm are observed in the magnified image (Figure 1f), which is conductive to improve the specific surface areas.

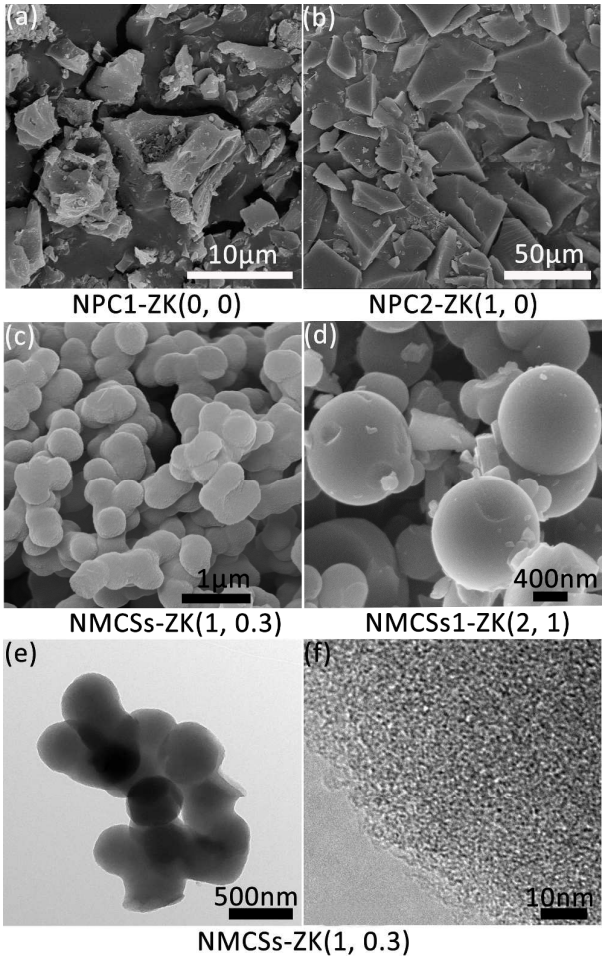

Figure 1. SEM images of (a) NPC1; (b) NPC2; (c) NMCSs; (d) NMCSs1 and TEM images of NMCSs (e-f) at different magnifications.

The porosity of the as-prepared NMCSs was further investigated by N_2 adsorption-desorption isotherm (Figure 2). The Brunauer-Emmett-Teller (BET) specific surface areas of NMCSs (1929 $m^2 g^{-1}$), NMCSs1 (1709 $m^2 g^{-1}$) and NPC2 (1993 $m^2 g^{-1}$) are much higher than that of NPC1 (426 $m^2 g^{-1}$), as listed in Table 1. Obviously, the higher surface area of NMCSs, NMCSs1 and NPC2 should be mainly due to the adding of $ZnCl_2$. The type I isotherm of NMCSs (Figure 2a) indicates that it contains mainly micropores (< 2 nm). The corresponding density functional theory (DFT) pore size distribution further shows that most of the pores have diameters less than 2 nm. It is already demonstrated that micropores with pore size either in the range of electrolyte ions or twice the size of electrolyte ions are much suitable for the formation of electrical double layer.[18] The formation of nano-pores in NMCSs and NPC2 system may be related to the reaction of $ZnCl_2$ and the neighboring carbon atoms at high temperature[27] or other possible mechanisms such as a template role to the added salt during the synthesis of NMCSs.[17] A small fraction of mesopores with pore diameter ranges of 2-3 nm was also observed. The results are well consistent with the above TEM observation.

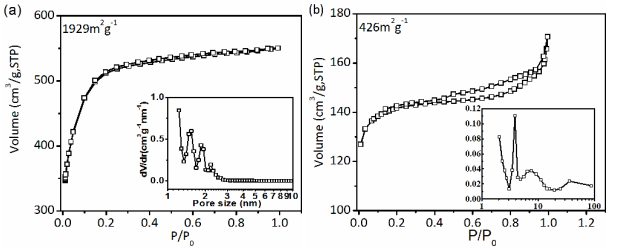

Figure 2. Nitrogen adsorption-desorption isotherms and pore-size distribution curve of (a) NMCSs and (b) NPC1, respectively.

Scanning TEM (STEM) and elemental mapping analysis of NMCSs proved the presence and uniform distribution of nitrogen，carbon and oxygen on the surface of NMCSs (Figure 3a). The XPS of C 1s and N 1s spectra in Figure 3c and 3d clearly indicate typically chemical character of carbon and nitrogen in NMCSs. The C1 peak at the bonding energy of 284.7 eV represents the graphite like C-C bond. The distinct peaks at 285.5 (C2) and 286.7 eV (C3) reflect two types of the C-N bonds, corresponding to the trigonal phase with a sp^2 bond and the tetrahedral phase with a sp^3 bond, respectively.[28, 29] Moreover, the high-resolution N 1s scan illustrated the presence of three forms of nitrogen on the surface of NMCSs. The peaks at bonding energies of 398.2 (N1), 400.0 (N2), and 401.1 eV (N3) are attributed to the pyridinic N, pyrrolic N, graphitic N in the carbon lattice, respectively.[27] According to previous studies,[12, 30] such high level of N1 and N2 in NMCSs are very beneficial to improve the capacitance performance, especially from the aspect of pseudocapacitance. Elemental mapping and XPS analysis also exhibit that small fraction of oxygen atoms are attached on the surface of NMCSs, which could be owing to moisture, atmospheric O_2 or CO_2 adsorbed on NMCSs as well as the residual oxygen-containing groups from TPAL (aldehyde group).[12, 31] It is widely accepted that the oxygen-containing functionalities on carbons contribute to the pseudocapacitance through the quinine/hydroquinone redox pair.[14]

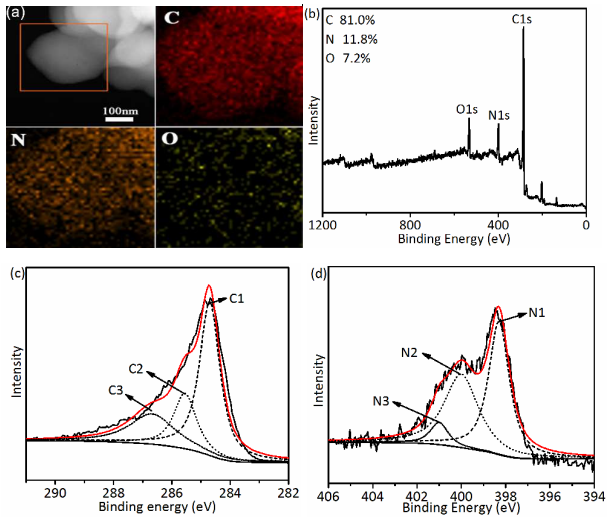

Figure 3. (a) STEM and the corresponding elemental mapping images of NMCSs; (b-d) XPS sweep scan, and the corresponding high-resolution XPS spectra of C 1s and N 1s of NMCSs.

The as-synthesized NMCSs have high nitrogen content, high surface area, and well-defined spherical morphology, making them ideal electrode materials for high-performance supercapacitor. Furthermore, the well-developed microporosity would interact strongly with electrolyte molecules, effectively enhancing the formation of electrical double layer, therefore increasing the capacitance value. In addition, the uniform nanospherical morphology of NMCSs can shorten the ion diffusion distance, allowing an easy entry of the electrolytes into the inner micropore system.[32]

In order to evaluate the electrochemical characteristics of the NMCSs, cyclic voltammetry, galvanostatic charge/discharge and electrochemical impedance measurements were carried out with a three-electrode system in 6 M KOH aqueous solution. Figure 4a and 4b show the cyclic voltammogram (CV) curves of NMCSs and NPC1 electrodes at different sweep rates. The CV curves of NMCSs have a rectangular-like shape even at a scan rate of 100 mV s^{-1}, displaying the representative electrostatic characteristic of EDLCs. The nitrogen and oxygen functional groups within NMCSs can induce pseudocapacitive effects and increase the accessibility of micropores by improving the wettability of the electrode surface.[33] Figure 4c and 4d shows the galvanostatic charge/discharge curves of the NMCSs electrode and the NPC1 electrode, respectively. It can be observed that the shapes of the charge/discharge curves are closely linear and symmetrical, indicating excellent capacitive behavior and electrochemical reversibility. The specific capacitances of the electrodes, C_s, were calculated from the galvanostatic charge/discharge curves using the following equation:

$$C_s = \frac{I}{(\Delta E / \Delta t)m} \qquad \text{Equation (1)}$$

Where 'I' is the discharge current, '(ΔE/Δt)' is the average slope of the discharge curve after the IR drop, 'Δt' is discharge time, and 'm' is active mass. The calculated specific capacitances of the NMCSs electrodes are 365, 293, 269, 247, 233 F g^{-1} at current densities of 0.5, 1, 2, 5, 10 A g^{-1}, respectively (Figure 5a). More interestingly, the capacitive value of NMCSs still retains 247 F g^{-1} at a high current density of 5 A g^{-1} suggesting that such a prominent capacitive performance can be maintained under a high power density operation. And the NPC2 and NMCSs1 electrodes show very similar specific capacitances with NMCSs. As a comparison, the NPC1 electrode has much lower specific capacitances of 234, 184, 161, 137, 127 F g^{-1} at current densities of 0.5, 1, 2, 5, 10 A g^{-1}, respectively, and NPC3 and NPC4 electrodes has even lower specific capacitances. Based on the above results, it could be found that $ZnCl_2$ plays a very important role in the formation of high specific surface area, which is crucial to the capacitance performance of electrode material. In contrast, KCl has negligible or even negative contribution to the capacitance improvement when too much was used. The remarkable specific capacitance of NMCSs is higher than many previously reported nitrogen-doped carbons, such as nitrogen-doped porous carbon nanofibers (202 F g^{-1} at 1 A g^{-1}),[34] terephthalonitrile-derived nitrogen-rich networks (250 F g^{-1} at 1 A g^{-1}),[35] nitrogen-enriched nonporous carbon materials (110 F g^{-1} at 0.1 A g^{-1}),[36] porous nitrogen-doped carbon nanotubes (210 F g^{-1} at 0.5 A g^{-1}),[37] hollow, spherical nitrogen-rich porous carbon shells obtained from a porous organic framework (230 F g^{-1} at 0.5 A g^{-1}).[38]

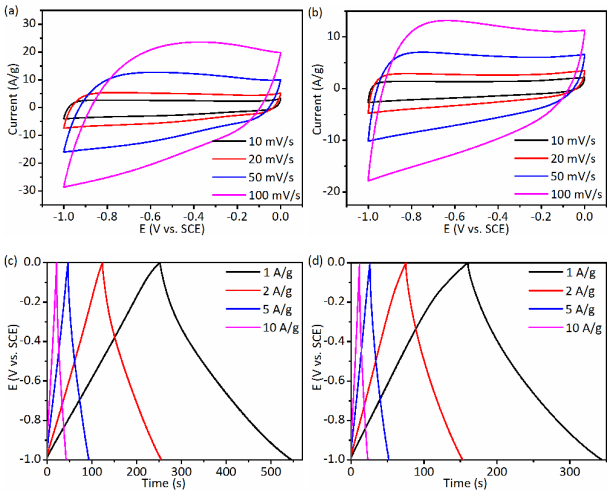

Figure 4. CV curves of (a) NMCSs and (b) NPC1 at different scan rates. Charge/discharge curves of (c) NMCSs and (d) NPC1 at different current densities.

Figure 5b shows the Nyquist impedance spectroscopy of NMCSs and NPC1, the nearly vertical lines in the low frequency region indicate that the electrodes show outstanding capacitor performance.[39] It is obvious that, the line of NMCSs is more vertical, indicating much better electrochemical capacitive properties The x-axis intercepts at high frequency in the Nyquist plots for NMCSs and NPC1 are 0.64 and 0.6, illustrating the low equivalent series resistances. A semicircle at the high to mid frequency region presenting the charge transfer resistance. A short 45° Warburg region at the middle frequency region shows the fast diffusion of the electrolyte ions.

Table 1: Summary of BET data and capacitance data

Samples	S_{BET} (m^2 g^{-1})	C_S (F g^{-1}) at 10 A g^{-1}
NPC1-ZK (0, 0)	426	123
NPC2-ZK (1, 0)	1992	220
NMCSs-ZK (1, 0.3)	1929	230
NMCSs1-ZK (2, 1)	1709	200

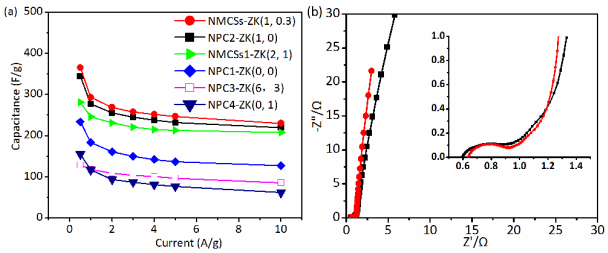

Figure 5. (a) Specific capacitance versus different current density. (b) Nyquist plots of NMCSs and NPC1 (NMCSs in red line, NPC1 in black line, the inset shows the spectra at high-frequency region).

The Ragone plots of NMCSs and NPC1 shown in the Figure 6a evaluate the performance of materials in terms of their energy density and power density. The energy densities (E) and power densities (P) were calculated using the following equations:

$$E=\frac{1}{2}\left(\frac{C_s}{4}\right)V^2 \qquad \text{Equation (2)}^6 \qquad P=\frac{E}{t} \qquad \text{Equation (3)}^6$$

where 'C_s' is the specific capacitance, 'V' is the maximum voltage and 't' is total discharge time. The NMCSs has a capability to deliver energy density of 8 Wh/Kg with a power density of 1377 W/Kg, when the power density decreases to 62 W/Kg, the energy density increased to 12 Wh/Kg,which is much higher than that of NPC1(8 Wh/Kg). To further evaluate the cycling stability of NMCSs, galvanostatic charge-discharge measurements were carried out at a current density of 3 A g^{-1} for 10000 cycles. As shown in Figure 6b, after 10000 cycles, the capacity decay is only 6% compared with the starting value, suggesting that the pore accessibility to electrolyte ions does not change greatly after long-term charge-discharge test and showing the excellent electrochemical stability and reversibility of the NMCSs electrode. The CV curves measured at a scan rate of 10 mV s^{-1} before and after the long-term charge-discharge measurements exhibit a similar rectangular-like shape without obvious change. The good cycling stability was attributed to the efficient ion and electron diffusion channel of NMCSs.

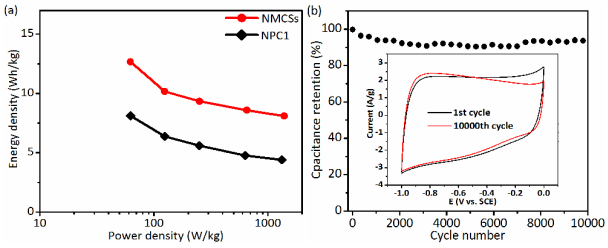

Figure 6. (a) Ragone plots of NMCSs and NPC1; (b) Cycling performance of NMCSs electrode at a current density of 3 A g^{-1} (The inset shows the CV curves at a scan rate of 10 mV s^{-1} before and after the cycling test).

4. Conclusion

In summary, NMCSs with both high surface areas and high heteroatom contents have been fabricated by a facile and cost-effective route. The use of molten salt not only avoids the complicated preparation process but also plays an important role in the formation of the well-developed microporous structure and spherical morphology. The NMCSs material has a high capacitance of 365 F g^{-1} at 0.5 A g^{-1} and retains 230 F g^{-1} at 10 A g^{-1} as well as good stability. Because of all these outstanding features, the resultant NMCSs are expected to be ideal candidates for high performance supercapacitors and other potential applications, such as catalysis, lithium ion batteries and so on.

Acknowledgements

This work was supported by the National Natural Science Foundation of China (Grant No. 21273114), the Natural Science Foundation of Jiangsu Province (Grant No. BK2012791), the Fundamental Research Funds for the Central Universities (Grant NO. NE2015003) and the "Six Talent Peaks Program" of Jiangsu Province (Grant No. 2013-XNY-010), a Project Funded by the Priority Academic Program Development of Jiangsu Higher Education Institution.

Notes and references

1. A. S. Arico, P. Bruce, B. Scrosati, J. M. Tarascon, W. V. Schalkwijk, *Nat. Mater.*, 2005, **4**, 366-377
2. M. Zhi, C. Xiang, J. Li, M. Li and N. Wu, *Nanoscale*, 2013, **5**, 72-88.
3. J. L. liu, H. J. Fan, Z. X. Shen, *Nano Lett.*, 2014, **14**, 7180-7187.
4. Y. Xu, Z. Lin, X. Huang, Y. Wang, Y. Huang and X. Duan, *Adv. Mater.*, 2013, **25**, 5779-5784.
5. S. Liu, S. Sun and X. Z. You, *Nanoscale*, 2014, **6**, 2037-2045.
6. N. Xiao, H. Tan, J. Zhu, L. Tan, X. Rui, X. Dong and Q. Yan, *ACS Appl. Mater. Interfaces*, 2013, **5**, 9656-9662.
7. D. Bhattacharjya and J. S. Yu, *J. Power Sources*, 2014, **262**, 224-231.
8. J. L. Liu, J. Sun, L. Gao, *J. Phys. Chem. C,* 2010, **114**, 19614–19620.
9. H. M. Jeong, J. W. Lee, W. H. Shin, Y. J. Choi, H. J. Shin, J. K. Kang and J. W. Choi, *Nano Lett.*, 2011, **11**, 2472-2477.
10. J. L. Liu, L. L. Zhang, Z. X. Shen, X. W. (David) Lou, *Energy Environ. Sci.,* 2014, **7**, 3709-3719.
11. Y. Zhu, S. Murali, M. D. Stoller, K. J. Ganesh, W. Cai, P. J. Ferreira, A. Pirkle, R. M. Wallace, K. A. Cychosz, M. Thommes, D. Su, E. A. Stach and R. S. Ruoff, *Science*, 2011, **332**, 1537-1541.
12. M. Zhou, F. Pu, Z. Wang and S. Guan, *Carbon*, 2014, **68**, 185-194.
13. J. Han, L. L. Zhang, S. Lee, J. Oh, K. S. Lee, J. R. Potts, J. Ji, X. Zhao, R. S. Ruoff and S. Park, *ACS Nano*, 2012, **7**, 19-26.
14. Z. Li, Z. Xu, H. Wang, J. Ding, B. Zahiri, C. M. B. Holt, X. Tan and D. Mitlin, *Energy Environ. Sci.*, 2014, **7**, 1708-1718.
15. J. Wang and S. Kaskel, *J. Mater. Chem.*, 2012, **22**, 23710.
16. Z. S. Wu, Y. Sun, Y. Z. Tan, S. Yang, X. Feng and K. Mullen, *J. Am. Chem. Soc.*, 2012, **134**, 19532-19535.
17. N. Fechler, T. P. Fellinger and M. Antonietti, *Adv. Mater.*, 2013, **25**, 75-79.
18. D. Puthusseri, V. Aravindan, S. Madhavi and S. Ogale, *Energy Environ. Sci.*, 2014, **7**, 728-735.
19. W. Yang, T. P. Fellinger and M. Antonietti, *J. Am. Chem. Soc.*, 2010, **133**, 206-209.

20. Z. Li, Z. Xu, X. Tan, H. Wang, C. M. B. Holt, T. Stephenson, B. C. Olsen and D. Mitlin, *Energy Environ. Sci.*, 2013, **6**, 871-878.
21. X. L. Wu, T. Wen, H. L. Guo, S. Yang, X. Wang and A. W. Xu, *ACS Nano*, 2013, **7**, 3589-3597.
22. R. Silva, D. Voiry, M. Chhowalla and T. Asefa, *J. Am. Chem. Soc.*, 2013, **135**, 7823-7826.
23. P. Pachfule, V. M. Dhavale, S. Kandambeth, S. Kurungot and R. Banerjee, *Chem. Eur. J.*, 2013, 19, 974-980.
24. X. Zhuang, F. Zhang, D. Wu and X. Feng, *Adv. Mater.*, 2014, **26**, 3081-3086.
25. X. Liu, N. Fechler and M. Antonietti, *Chem. Soc. Rev.*, 2013, **42**, 8237-8265.
26. X. Liu, Giordano C, M. Antonietti, *Small*. 2014, **10**, 193-200.
27. H. Zhu, J. Yin, X. Wang, H. Wang and X. Yang, *Adv. Funct. Mater.*, 2013, **23**, 1305-1312.
28. Y. Wang, X. Cui, Y. Li, L. Chen, H. Chen, L. Zhang and J. Shi, *Carbon*, 2014, **68**, 232-239.
29. S. Ratso, I. Kruusenberg, M. Vikkisk, U. Joost, E. Shulga, I. Kink, T. Kallio and K. Tammeveski, *Carbon*, 2014, **73**, 361-370.
30. X. Yang, D. Wu, X. Chen and R. Fu, *J. Phys. Chem. C*, 2010, **114**, 8581-8586.
31. P. Zhang, F. Sun, Z. Xiang, Z. Shen, J. Yun and D. Cao, *Energy Environ. Sci.*, 2014, **7**, 442-450.
32. Z. Li, D. Wu, Y. Liang, R. Fu and K. Matyjaszewski, *J. Am. Chem. Soc.*, 2013, 2014, **136**, 4805-4808.
33. Z. Y. Jin, A. H. Lu, Y. Y. Xu, J. T. Zhang and W. C. Li, *Adv. Mater.*, 2014, 26, 3700-3705.
34. L. F. Chen, X. D. Zhang, H. W. Liang, M. Kong, Q. F. Guan, P. Chen, Z. Y. Wu and S. H. Yu, *ACS Nano*, 2012, **6**, 7092-7102.
35. L. Hao, B. Luo, X. Li, M. Jin, Y. Fang, Z. Tang, Y. Jia, M. Liang, A. Thomas, J. Yang and L. Zhi, *Energy Environ. Sci.*, 2012, **5**, 9747-9751.
36. D. Hulicova-Jurcakova, M. Kodama, S. Shiraishi, H. Hatori, Z. H. Zhu and G. Q. Lu, *Adv. Funct. Mater.*, 2009, **19**, 1800-1809.
37. G. Xu, B. Ding, P. Nie, L. Shen, J. Wang and X. Zhang, *Chem. Eur. J.*, 2013, **19**, 12306-12312.
38. X. Liu, L. Zhou, Y. Zhao, L. Bian, X. Feng and Q. Pu, *ACS Appl. Mater. Interfaces*, 2013, **5**, 10280-10287.
39. S. M. Dong, X. Chen, L. Gu, G. L. Cui, L. Q. Chen *Energy Environ. Sci.*, 2011, **4**, 3502-3508.

Graphical Abstract

Schiff-Base Polymers Derived Nitrogen-Rich Microporous Carbon Spheres Synthesized by Molten-Salt Route for High-performance Supercapacitors

Shanjin Su, Qingxue Lai and Yanyu Liang*

College of Materials Science and Technology, Nanjing University of Aeronautics and Astronautics, 210016 Nanjing, (P.R. China)

*Corresponding author. Tel: +86 25 52112626; Fax: +86 25 52112626.

E-mail address: liangyy403@126.com

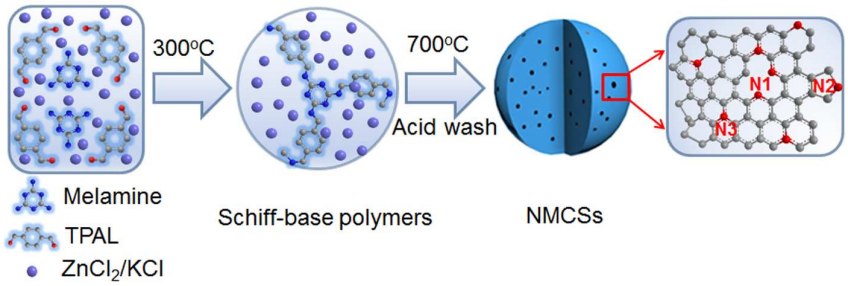

Molten-salt route and Schiff-base chemistry are combined to prepare nitrogen-rich microporous carbon spheres. The as-prepared microporous carbon materials show excellent capacitive performance and stable cycle life as electrode materials for electrical double layer capacitors. With regard to the simple and environmental-friendly synthetic route, it holds great potential for the industrial manufacture of microporous carbon materials.